An investigation into the spectral parameters of ULF waves in the polar caps and magnetotail

Nataliya Sergeevna Nosikova[1,2], Nadezda Viktorovna Yagova[2], Lisa Jane Baddeley[3], Dag Arne Lorentzen[3], Dmitriy Anatolyevich Sormakov[4]

[1]National Nuclear University "MEPhI", Moscow, Russia

[2] Schmidt Institute of Physics of the Earth of the Russian Academy of Sciences (IPE RAS), Moscow, Russia

[3]University Center on Svalbard, Norway

[4]Arctic and Antarctic Research Institute, AARI, Geophysics department, Sankt-Petersburg, Russia

Correspondence to: Nataliya S Nosikova (NSNosikova@mephi.ru)

Abstract.

The present case study is focused on fluctuations at ~1.5 mHz observed at open field lines, in the both polar caps in ground-based geomagnetic data and in electron concentration in the northern hemisphere ionosphere. Coherent pulsations with a relatively narrow Pc-like spectra and a higher fraction of the transversal components in the total spectral power are also observed by the Cluster satellites in the magnetotail magnetic field. Interestingly, the pulsations in the magnetotail started after pulsations over a similar frequency range observed in the solar wind dynamic pressure and IMF had been switched off. This suggests evidence of an internal, resonant magnetotail mode which is normally masked by a higher amplitude broadband ULF "noise" of extra-magnetospheric origin.

1 Introduction

One of the most important mechanism of energy transfer in the Magnetosphere is through the propagation of Ultra Low Frequency (ULF) waves. Of particular interest are intensive, high latitude geomagnetic pulsations at mHz frequencies (Pc5/Pi3). These pulsations are the most long-period and intensive magneto-hydrodynamic (MHD) waves in the magnetosphere. Their longest possible period is determined by the magnetosphere size to Alfven velocity ratio and is about 10^3 s. Contribution of ULF waves into the solar-wind magnetosphere interaction is quantified by ULF wave indexes (e.g. Kozyreva et al., 2007, Borovsky and Denton, 2014). The highest Pc5/Pi3 amplitudes correspond to auroral latitudes (Baker et al., 2003). Specific ULF activations were found near the polar boundary of the auroral oval and associated with polar boundary

intensifications (PBIs) (Lyons et al., 1999). The other region of high Pi3 intensities is collocated with the cusp/cleft region (Bolshakova and Troitskaya, 1977; De Lauretis et al., 2016). Meanwhile, Pc5/Pi3 are observed in the polar caps, where field lines are "open". They are characterized by lower amplitudes (in comparison to auroral Pc5 pulsations which can result from Alfven field-line resonance (FLR) on closed field lines) and are more irregular with typically lower central frequencies ~ a few mHz (Bland and McDonald, 2016). A detailed analysis of morphological properties of these pulsations can be found in (Yagova et al., 2004; Francia et al., 2005). These pulsations are simultaneously seen in geomagnetic and radar data and might be directly driven by perturbations in the SW, be related to substorms or be a result of internal processes in the magnetosphere. The polar cap pulsations are coherent at long distances (Yagova et al., 2004). This indicates that an external source of these pulsations should exist. Kepko et al. (2002) suggested that the primary cause of global magnetospheric pulsations is ULF perturbations in the pressure and density of the Solar Wind (SW). In some cases, these pulsations are literally global. Thus Han et al. (2007) reported on low latitude observations of global Pi3 pulsations directly driven by fluctuations in the SW. A contribution of the main SW/IMF pulsations to the spectral power of polar cap Pi3s was estimated by Yagova et al. (2007) who showed that the amplitudes of polar cap Pi3s and fluctuations of IMF SW dynamic pressure in the same frequency range correlate not only for high amplitude wave packets but at any intensity of extra-magnetospheric fluctuations. Later, Kepko et al. (2020) carried out a detailed analysis of long-term observations of quasi-periodical spatial mesoscale irregularities in the SW number density. The authors have shown that at least some of the frequencies of global pulsations in mHz range can originate from the meso-scale SW structures. If the ULF variations in the SW are neglectable, pulsations might result from exciting Kelvin-Helmholtz instability in the magnetosphere (Mann et al., 2002, Rae et al., 2005, Keiling 2009).

Inside the magnetosphere, the spectral parameters of ULF waves can be determined by spectral characteristics of disturbances outside the magnetosphere along with the waveguide and resonance properties of the magnetosphere-ionosphere system (e.g., Alperovich and Fedorov, 2007). In particular, it has been shown that ULF spectra at polar cap latitudes are not totally controlled by the parameters in front of the bow shock but are a manifestation of processes in the magnetosphere and magnetosheath (Yagova, 2015). Pilipenko et al. (2005) theoretically showed, that an Alfven quasi-resonator can be formed on open field lines due to the curvature of the magnetic field. This mechanism can provide one explanation ULF activity observed in the polar cap.

As polar caps are projections of the geomagnetic tail lobes, existence of specific tail modes was discussed by (Allan and Wright, 2000). Cluster observations showed low average amplitudes of ULF in the tail lobes, as well as weak correlation of ULF power in both Pi2 and Pc5 frequency bands with auroral activity (Wang et al., 2016). Zhang et al. (2018) used ion velocity data to identify ULF waves and analyzed how substorm activity influences wave occurrence and the main frequency. They found that the Pc5 frequencies differ for non-substorm and substorm waves. Ballatore (2003) analyzed statistically integral parameters of ULF power in Pc5 range at two nominally conjugated positions. In both papers mentioned above there was no information about pulsation waveforms or coherence. An important evidence of interrelation between ULF activity in the polar cap and at auroral latitudes was found by (Bland and McDonald, 2016) who studied high latitude ULF waves under

59 quiet geomagnetic conditions. The authors found that polar cap ULF waves were accompanied by simultaneous activity in the
60 dayside auroral zone at nearly the same frequency (1-1.3 mHz).

61   However, there are only a few publications on conjugated observations of ULF waves in the magnetotail and one or
62 both polar caps or between two hemispheres at cap latitudes. This is partly because of low amplitudes of polar cap Pi3s which
63 are usually masked by more intensive directly driven fluctuations seen simultaneously throughout the high latitude region.
64 The other source of contamination is associated to PBIs (Lyons et al., 1999; 2011). The inter-relations between the auroral
65 activations, PBIs and auroral phenomena in the polar caps was studied by Nishimura et al. (2013; 2014). Although a substorm
66 is mostly an auroral phenomena, it causes essential changes in/across the whole night-time magnetosphere and is followed by
67 auroral and geomagnetic disturbances in the polar caps. The oscillations in the Pc5/Pi3 range caused by a substorm in polar
68 cap particle precipitation was reported in (Weatherwax et al., 1997). Pre-substorm variations of polar cap ULF activity were
69 reported in (Heacock and Chao, 1980; Yagova et al, 2000; 2017). Shi et al. (2018) summarized previous studies of long-lasting
70 poloidal ULF waves in the Magnetosphere including their own investigation. It is seen from Table 1 in (Shi et al., 2018) that
71 the mean duration of the event is 2-3 days, and pulsations are detected on the dayside or from the dayside to midnight. The
72 authors pointed out that "the waves were usually monochromatic and observed during low geomagnetic activity after a
73 geomagnetic storm or within the storm recovery phase". Later, (Shi et al., 2020) concentrated on one event from those studied
74 in (Shi et al., 2018). The authors reported long-lasting Pc5 pulsations from L~5.5 and up to the polar caps in both hemispheres
75 seen simultaneously in the ground-based magnetometer and SuperDARN radar data. At the same time, pulsations were
76 detected by MMS satellite in the Magnetosphere. Their study indicated that the Pc5 pulsation observed under the quiet external
77 parameters and within the storm recovery phase at closed and open field lines were from the same source.

78   The present case study is focused on a long-lasting pulsation which took place 08.08.2007 and was recorded
79 simultaneously in the magnetotail and in both polar caps. While ULF fluctuations almost die out in the SW and IMF, ULF
80 activity starts to grow and become more coherent in the magnetosphere as shown from both the Cluster and ground
81 magnetometer data in the both polar caps. To minimize possible influence of both extra-magnetospheric fluctuations and
82 residual activity related to the recovery phase of a geomagnetic storm (Posch et al., 2003) or recent substorm activations, an
83 interval with a quiet conditions both in the interplanetary space and in the magnetosphere have been chosen using the same set
84 of parameters as in (Yagova et al., 2017).
85

2 Data processing

2.1 Data

Data from the IMAGE magnetometer network, VOS, DVS, DRV, THL magnetic stations, EISCAT radar, CLUSTER, DMSP as well as OMNI Solar wind and IMF data were utilized. The position of the Cluster satellites and the field line projection of their position (between 12 and 18 UT) together with the location of the stations are given in Figure 1. It should be noted, that the both satellites were in the tail Southern tail lobe for the full day (not shown).

IMAGE is a European magnetometer network equipped with three-component flux-gate magnetometers with 10 s initial time resolution (Tanskanen, 2009). The chain is located approximately along the magnetic meridian 100 (MM100), and it covers CGM latitudes from $\Phi=77°$ to $40°$. Information on the stations utilised in this study and their coordinates is presented in Table 1.

The EISCAT Svalbard radar (ESR) is co-located with the LYR magnetometer station ($\Phi=75.4°$) and can make detailed measurements of ionospheric electron density, electron temperature, ion temperature and ion line-of-sight velocity. The radar operates in the 500 MHz band with a peak transmitter power of 1000 kW. In the present paper, data from the 42-meter dish (field aligned pointing position) taken during the International Polar Year (2007–2008) are used.

To map the magnetic field variations from the magnetotail to the ground, data from Cluster satellites fluxgate magnetometer have been included (Balogh et al., 1997). The values of footprint coordinates are taken from https://sscweb.gsfc.nasa.gov/cgi-bin/Locator.cgi. The Tsyganenko 89C model is used for field line tracing

On the 8th of August 2007 (day 220) all four Cluster satellites were located in the southern tail lobe at radial distances of between 15 to 20 Re. Specifically, fluxgate magnetometer data from Cluster 1 and 3 are used (which had a separation distance of approximately 1 R_E along the Sun-Earth line). Using the TS01 model, Cluster 3 was nearly conjugated with the DRV station (its southern footprint at 17:10 UT was at -68.7°, 141.4° geographic and -76°, 236° CGM).

2.2 Data Processing

Preliminary data processing includes band-pass filtration in the frequency band 0.8-8.3 mHz and decimation to a common 1minute temporal resolution. The lower frequency of the filter window corresponds to ~ 20 min period. An example of spectra of a non-filtered signal can be found in the Figure S1 in the supplementary materials. All spectral maxima at frequencies above 1.1 mHz are separated from the filter-related maxima in all the spectra shown as examples and used in statistical analysis.

In the case of the magnetospheric satellite measurements of the magnetic field, a local field-aligned system is used. For each time instant, there are two magnetic field vectors in GSE coordinate system, i.e., the instantaneous vector **B** and the averaged over the time window one $\mathbf{B}_{av}$. The field aligned component $B_{//}$ is defined as a projection of **B** to $\mathbf{B}_{av}$. The radial component B_ρ is normal to $\mathbf{B}_{av}$ and lies in the plane containing **B** and the Earth centre and directed downward. The azimuthal component B_φ is normal to both $B_{//}$ and B_ρ: its direction is determined from the condition that three components form a right-hand triangle.

Electron concentration registered by the EISCAT radar are preliminarily sliced with height, averaged, and passed through the low-band filter with a cutoff frequency f_c=8.3 mHz. On the day of the case study, 8th August, Svalbard was experiencing the midnight Sun period so the level of background solar radiation incident on the ionosphere was high. Nevertheless, variations of electron density (ΔN_e) are suitable for analysis.

The processing of all data (ground and space based) to a common temporal resolution allows a cross-spectral analysis to be performed between the various data sets. The Blackman-Tukey method (Jenkins, 1969; Kay, 1988) is applied to obtain a power spectral density (PSD) for each variable, along with PSD ratio (R), spectral coherence (γ^2) and phase difference ($\Delta\varphi$) for each pair of variables. The spectra are calculated in a 96-points (5760 s) sliding window with an 8-min shift between subsequent intervals. Whilst the Blackmann-Tukey method has a more course frequency resolution than other similar methods (such as the Maximum Entropy method), it estimates the PSD with a dispersion which decreases with spectral smoothing.

The spectral estimation parameters were chosen as a compromise between two opposite requirements, namely a better frequency resolution and a lower dispersion of the spectral estimation. It should be remembered that the dispersion of spectral coherence and phase difference depends on the absolute value of coherence and goes to zero at $\gamma^2 \to 1$.

OMNI data (time delayed to the Bow Shock) are used for spectral estimations in the IMF whilst Cluster data are used for the magnetotail. Various studies have looked at the response time of the magnetosphere to changes in the Solar Wind (primarily to changes in the IMF). Wing et al. (2002) found a the nightside response time to changes in the IMF of ~12 minutes (at geosynchronous orbit). Given that this study is looking at pulsations with a periodicity of ~12 minutes (1.5 mHz) and using a 1.5-hour sampling window for PSD and coherence estimates then the OMNI data has not undergone any additional time lag when evaluating the coherence between that and the Cluster data.

3 Results of the analysis

3.1 Space weather conditions and ground based magnetometers data on day 220 2007

The magnetic field data from the TRO and BJN stations and AE-index, as well as IMF and SW parameters are shown in Figure 2, left panel. It is seen from the Figure, that the IMF was undisturbed, and the absolute value of the B_Z component hardly exceed 3 nT. The absolute value of the solar wind speed V was slightly decreasing for the entire period and the mean value was about 500 km/s, which corresponds to moderate SW. The SW dynamic pressure stayed low and there were no rapid changes. The AE index was increasing from 14 UT to 16 UT and there were two enhancements: around 17 UT, and at 20:30 UT. The second enhancement, at 20:30 UT, marked with the vertical blue arrow, corresponds to a substorm. Although the magnitude of the substorm bay is small (~100 nT), observations by DMSP-satellite (F16, Figure 2b, top right panel) indicate auroral enhancements consistent with a substorm (i.e., particle precipitation occurring from the magnetotail). It should be

146 added that there is no ground based optical observations available in the high latitude northern region due to 24-hour daylight
147 conditions in northern Scandinavia.

3.2 ULF fluctuations on the ground and in space

149 In this section, the analysis of ULF fluctuations in interplanetary space, the magnetotail and on the ground are presented. The
150 parameters of the IMF/SW fluctuations and geomagnetic pulsations in the magnetotail are calculated throughout the day to
151 illustrate how the parameters of the pulsations in the magnetotail and on the ground are controlled by extra-magnetospheric
152 parameters and the changing (i.e., moving from the auroral oval to the polar cap) of the magnetospheric projection of ground
153 stations. Such a time scale is used in Figures 4(a),6, 8, and 10. For a more precise analysis of the pulsation spectral properties,
154 a shorter time interval is used in Figures 4(b, c), 11, 12, and 14.

3.2.1 Geomagnetic pulsations on the ground: Northern hemisphere

156 ULF pulsations are observed in the ground magnetometer data stations located on Svalbard (from NAL to HOR) and at BJN
157 and become indistinct at TRO station, situated on the mainland (Figure 3). For the ground stations, the notations B_N and B_E
158 are used for the components oriented northward along the magnetic meridian, and eastward (orthogonal), respectively. The
159 time series starts at 15:00 UT and stretches for 180 minutes. The maximal amplitude reaches ~25 nT peak to peak at ~16:30 UT
160 for LYR and NAL and then decreases for the value of a few nT.
161 The diurnal variations of the Pi3 (1-4 mHz) power at NAL is controlled by two active regions: the polar cusp, which is
162 responsible for near-noon activity, and the polar boundary of auroral oval in the morning and evening MLT sectors (see Yagova
163 et al. (2004) for details). The station crosses both zones at different UTs with a dependence on seasons and geomagnetic
164 activity in the morning and afternoon MLT sectors. The PSD variation during the day analysed is shown in Figure 4(a). Each
165 data point along the time axis in Figure 4 (b) corresponds to a starting point of a nearly 1.5-hour (96 minute) interval. After
166 the cusp-related maximum near MLT noon (UT=9) (indicated by the vertical red arrow), the PSD reaches a maximum at 13
167 UT (16 MLT) (indicated by the vertical purple arrow). Afternoon Pi3s, seen after 15 UT, do not relate to the cusp activity and
168 are the object of our special interest.
169 To clarify how the contribution of polar cap and auroral oval activity to the NAL pulsations changes with time, the variation
170 of the Pi3 PSD ratio, R, and spectral coherence, γ^2, for THL-NAL and HOR-NAL station pairs are given on right (Figure 4,
171 b-c). HOR is located ~ 3 degrees southward from NAL on the MM100 chain, while THL lies at $\Phi=84.84°$, i.e., deep in the
172 polar cap. Although THL is shifted by 5.5 hours in MLT from the MM110 stations, the diurnal variation is almost negligible
173 for this location (Yagova et al., 2010) and this station can be taken as an indicator of condition in the polar cap. As it was
174 shown (Yagova et al., 2017), the main pulsation power is concentrated in the frequency band from 1.25 to 1.9 mHz, and UT
175 from 8 to 20, i.e., from pre-noon to almost midnight in MLT. It is seen from the Figure 4b, that both the THL/NAL and
176 HOR/NAL PSD ratio, $R < 1$, at near-noon hours, i.e., NAL is dominating, probably due to cusp-related activity. From 11 to

177   16:30 UT, the THL/NAL spectral ratio, $R > 1$, while HOR/NAL spectral ratio, $R \sim 1$, i.e., the PSD deep in the polar cap is

178   maximal. The HOR/NAL PSD ratio then grows while the THL-NAL PSD ratio remains at ~1. From 13 to 17 UT, the pulsations

179   are coherent for both the THL-NAL and HOR-NAL station pairs with coherence maxima at 14 and 16 UT (Figure 4c). For the

180   first maximum, the HOR-NAL spectral coherence is higher, while for the second one the coherence for the THL-NAL station

181   pair exceeds that for HOR-NAL. This means that after 15 UT, the polar cap (THL) pulsations demonstrate both the highest

182   PSD and coherence with those at NAL. This effect can be associated with NAL moving from the auroral oval to the polar cap

183   or can also result from temporal variations of the pulsation parameters, such as PSD distributions along a meridian and/or

184   spectral coherence.

185   An example of the B_N component variations and their spectral parameters are presented in Figure 5. The left panel (Figure 5a)

186   shows a time series of the B_N component from 15:4417:20 UT from the NAL, THL and HOR stations. The pulsation has a

187   period of approximately 11 minutes (~1.5 mHz) and the peak-to-peak amplitude is about 25 nT at NAL and THL, and ~15 nT

188   at HOR.   Note, that the lower frequency of the filter f_L=0.8 mHz corresponds to ~20 min period which is almost twice longer

189   than the main pulsation's period. Figures 5b – 5d show the (b) PSD in each location, (c) the interstation spectral coherence,

190   and (d) phase difference. The main maximum of the PSD at all the stations is found at f_1=1.5 mHz and the value of the PSD

191   decreases with CGM latitude from THL to HOR (Figure 5b). This spectral coherence for both the NAL-THL and the NAL-

192   HOR station pairs also demonstrate a maximum at $f= f_1$ (as is shown in Figure 5c). Note, that the spectral coherence between

193   NAL and THL (green line in figures 5c and 5d) is higher, than between NAL and HOR (blue line in Figures 5c, d). The

194   pulsations at NAL and THL are almost in phase in the vicinity of f_1, while a phase difference of $\sim\pi$ exists between NAL and

195   HOR. To summarize, the pulsations in the polar cap are characterised by a clear spectral maximum, and the only difference

196   from typical auroral Pc5s, is a lower frequency of the main maximum (f_1=1.5 mHz).

197   **3.2.2   Magnetic   pulsations   in   the   magnetotail   and   interplanetary   space**

198

199   It is commonly believed that the pulsations in the polar caps are directly driven by fluctuations in the SW. To find a source of

200   the studied pulsations, ULF disturbances in the SW, IMF, magnetotail and ionosphere were analysed. The average PSD and

201   coherence of magnetic field fluctuations in the IMF, calculated from OMNI, and in the magnetotail, recorded by Clusters 1

202   and 3, are presented in Figure 6 (over the same frequency range, 1.2–1.9 mHz, as those presented in Figure 4). The variations

203   in PSD of the three IMF components and field aligned component $b_{\parallel}$ in the magnetotail (Cluster3) are given in Figure 6a. One

204   can see from the Figure, that the spectral power in the IMF decreases rapidly at about 13.30 UT (black, dashed arrow in the

205   Figure), and then at ~15 UT the decrease is seen in the magnetotail (black solid arrow in figure 6a). Figure 6(b) shows the

206   corresponding PSD in the SW dynamic pressure, P_{SW}, and density, n.   Whilst there is an increase in spectral power from

207   10 – 15 UT, there is a sharp decrease at 15 UT, i.e., nearly simultaneously with that of the magnetic field in the magnetotail.

208 Simultaneously, the coherence between the pulsations, as measured by Cluster 3 and Cluster 1, in the magnetotail (Figure 6c)
209 jumps almost to unity, while no severe changes in IMF-Cluster coherence occur. In the coherence panel (figure 6c), only the
210 X-component of IMF is shown as the coherence variations between the Cluster field aligned component, and Y and Z IMF
211 components are similar to the Cluster – IMF b_X coherence. However, the latter demonstrates a closer agreement to the
212 coherence variations within the magnetotail before the pulsation regime changed at about 15 UT (magenta curve in Figure 6c).
213 A similar decrease is found in the coherence between the magnetic field in the magnetotail and P_{SW}, fluctuations (Figure 6d).
214 As the fluctuations of SW density and dynamic pressure were almost identical ($\gamma^2 \sim 1$), only the coherence variations between
215 P_{SW} and Cluster 3 are shown in Figure 6d.
216 The change of pulsation regime in the magnetotail is rather abrupt and it can be seen in the time domain as well. Figure 7
217 shows the pulsations in $b_\parallel$ registered simultaneously at Clusters 1 and 3 and their PSD spectra. The time series for the interval
218 started at 15:04 UT is given in Figure 7a. The switch from more or less similar pulsations to almost identical ones is seen at
219 about 15:30 and marked with an arrow. The PSD spectra for the interval started at 15:44 (Figure 7b) has the main spectral
220 maximum at f=1.5 mHz, i.e., at the same frequency f_1, as observed by the ground magnetometers.
221 To quantitively describe the variation of the spectral shape of the magnetotail pulsations during the day we have used the
222 method described by Yagova et al. (2010, 2015). The technique is based upon an expansion of the function $\sigma(F)$ (a log-log
223 spectrum, where σ and F are the logarithms of PSD and frequency, respectively) into Ledgrendre polynomials with the
224 resulting first 3 coefficients (L_0, L_1, L_2) providing the required quantitative description. In particular, the Q parameter is used
225 (where Q=-L_2), which estimates the deviation of the spectrum from an inverse power approximation (colour noise) near the
226 central frequency of interest.
227 The results for the Q-parameter analysis, along with the spectral power ratio and phase difference between the different
228 magnetic field components in the magnetotail, as measured by Cluster 3 are shown in Figure 8. The Q value increases rapidly
229 for all 3 components ($b_\parallel$, b_φ and b_ρ) after the PSD in the IMF decreases (i.e., after the switch off of the mHz fluctuations in the
230 IMF (dash-dot arrow at about 13.30 UT) and it reaches maximal value at 15 UT. It should be noted that at 15 UT, the PSD in
231 the SW pressure decreases rapidly, however, the Q value for the $b_\parallel$ and b_ρ magnetic field components in the magnetotail
232 remains high ($Q > 0.5$) until 18 UT (and until 17 UT for the b_φ component). For $b_\parallel$, Q slowly fluctuates between -0.5 and 0.5
233 from 0 at 13 UT and afterwards reaches almost 1 within half an hour. The growth for the transversal components (b_φ and b_ρ)
234 after 13:30 UT is not as fast, and Q reaches its maximal value after 15 UT.
235 It has been shown by Pilipenko et al. (2013) that the characteristics of the magnetotail are highly sensitive to the polarization
236 parameters of the pulsations (in comparison to a simple amplitude based investigation). The wave polarisation characteristics
237 were changing during the interval analysed, as seen from the variations of the spectral power ratio, R, and phase difference,
238 $\Delta\varphi$, for the $b_\parallel b_\rho$ and the $b_\parallel b_\varphi$ component pairs (Figures 8b and 8c). For both pairs of components, R exceeds unity almost all
239 day long, i.e., the compressional component is dominating. The only exceptions are registered at 3, 8, and 15 UT. In the
240 afternoon MLT sector, i.e., after 9 UT, it first increases from 2 to nearly 10 and then drops to 2 for the $b_\parallel b_\rho$ and below unity

241 for the $b_\parallel b_\varphi$ component pairs. Between 1518 UT the average R value is 2-3 times lower than for the previous 3 hours. Averaged

242 over the same frequency band, the sin of the inter-component phase difference, $\Delta\varphi$, is shown at the bottom panel. Before 15

243 UT, the parameter varies predominantly in the interval [-0.5, 0.8] and it differs for two component pairs. At 15 UT it changes

244 to almost unity for both component pairs. This corresponds to $\pi/2$ phase difference between field aligned and each of

245 transversal components, indicating a large-scale pulsation with a high fraction of transversal (Alfven) components. The interval

246 of $\pi/2$ phase difference and low R values are seen in Figure 8 from 15 till 18 UT, i.e., it coincides with the interval of low

247 amplitude, high Q and spectral coherence of Pi3 pulsations in the magnetotail.

3.2.3 ULF waves in the magnetotail and on the ground: Inter-hemispheric relationship

249 Since the Cluster satellites were in the southern tail lobe, only a footprint in the Southern polar region can be calculated. To

250 understand, how the magnetotail pulsations are related to those recorded in the two polar cap ionospheres, the pulsations

251 recorded at Cluster have been compared with those, recorded in the Southern Polar cap, and the latter with the Northern polar

252 cap pulsations. A time series of the pulsations registered simultaneously in the magnetotail at Cluster 3 and in both polar cap

253 ionospheres are presented in Figure 9 (a-c) and the spectral coherence for the pairs of components (1 ground, 1 magnetotail)

254 are given in panels (d-f). Pi3s at the DRV station, which is nominally conjugated with Cluster-3 during this time period, have

255 a peak-to-peak amplitude of about 2 nT (Figure 9a), and the maximal spectral coherence, γ^2, at 1.5 mHz (f_1) exceeds 0.9 for

256 both field-aligned and transversal components (Figure 9d). It is the maximal value among all the satellite-ground pairs.

257 Pulsations at the VOS station, located deep in the southern polar cap, are similar to the pulsations at Cluster-3 and at DRV.

258 Their peak-to-peak amplitudes reach 4 nT (Figure 9b). The Cluster3-VOS spectral coherence for both components at VOS and

259 the field-aligned component at Cluster-3 is shown in Figure 9e. It reaches a spectral coherence of 0.7 at the frequency, f_1 and

260 is higher than the coherence between the pulsation at VOS and the transversal components at Cluster (not shown here). During

261 this interval, the ground Pi3s are more intensive in the Northern than in the Southern hemisphere. Hence, the peak-to-peak

262 amplitude at NAL is about 25 nT (Figure 9c). The maximal coherence, $\gamma^2 \approx 0.9$, between the NAL and Cluster pulsations is

263 found for the b_ρ-b_N component pair (Figure 9f). The results show that there is clearly a high coherence between the pulsations

264 observed in the magnetotail and those in the polar cap ionospheres.

265 A time series of spectral power and coherence, in the 1.2 – 1.9 mHz frequency band, for different pairs of components for

266 Cluster 3 and VOS is presented in Figure 10. The VOS station is taken, because it is located deep within the polar cap at any

267 local time, and thus the influence of the cusp and auroral activity is minimal. A decrease of spectral power at VOS starts

268 immediately after the "switch off" of IMF fluctuations (this instant dash-dot arrow in Figure 10). However, the total decrease

269 of spectral power in the ionosphere is not so severe as in the magnetotail. From 15UT (marked by the black solid arrow) the

270 spectral power measured at VOS remains approximately constant, despite the fact that the spectral power at both Cluster and

271 in the SW dynamic pressure (P_{SW}) (Figure 6b) has decreased significantly. As a result, the tail to ground (T-G) spectral power

272 ratio R_{T-G} during the interval 15-18 UT is high in comparison with the previous hours (Figure 10b). The spectral coherence is
273 also higher than its average value during the day, especially for the $b_{\parallel}$ (Cluster)- b_N (VOS) component pair (Figure 10c).

274 A time series of spectral coherence, in the 1.2 – 1.9 mHz frequency band, between Cluster 3 and 4 ground-based stations in
275 the both hemispheres is shown in Figure 11. The DRV station is nominally conjugated to Cluster-3, the NAL station is located
276 in the Northern hemisphere, VOS and THL are placed deeper in the southern and northern polar caps respectively as it was
277 mentioned above. The three columns of the Figure 11 correspond to the three magnetic field components in the magnetotail,
278 and four rows to the four stations. The two g round horizontal magnetic components are colour coded with b_N in green and b_E
279 in orange. The time interval from 8 to 20 UT corresponds to hours from local noon to midnight at the TRO station. The highest
280 coherence is found for the b_N (DRV)-b_{φ} (Cluster-3) component pair and last for 2 hours from 15 to 17 UT. During the interval,
281 a large-scale pulsation with a high fraction of transversal (Alfven) components in the spectral power is recorded in the
282 magnetotail. A high ($\gamma^2=0.7$) but short coherence maximum is seen also in b_N (DRV)-$b_{\parallel}$ (Cluster-3) component pair. A similar
283 to b_N (DRV)-b_{φ} (Cluster-3) time evolution is found for the b_E (VOS)-$b_{\parallel}$ (Cluster-3) and b_E (VOS)-b_{φ} (Cluster-3) component
284 pairs, but at somewhat lower absolute values of γ^2. As it is seen from the bottom two rows of panels, during the 15-17 UT time
285 interval, the averaged coherence hardly exceeds 0.5 for all components Cluster 3 - NAL and Cluster 3 - THL, i.e., for stations,
286 located in the Northern polar cap. Generally, the averaged coherence between magnetotail Pi3s with those observed in the
287 northern polar cap is lower than that for the Southern polar cap, as is expected as the Cluster satellites are located in the
288 Southern tail lobe.

289 The inter-relation between the pulsations in the polar caps cannot be completely described by their spectral coherence with the
290 only a single location on open field lines, in the magnetotail. It seems possible to partly compensate for this with the analysis
291 of the coherence between the two polar caps and within each cap. Since the ionospheric observations are available in the
292 Northern hemisphere at the NAL longitude (see table 1), all possible pairs of horizontal components for two combinations of
293 stations (VOS-DVS in the Southern hemisphere, and DVS-NAL between the two hemispheres) were analysed. It should be
294 noted that the maximal coherence at high latitudes is possible not only for the corresponding components (Lepidi et al., 1996).
295 Hence, a maximal coherence can be found for two polar cap stations not between both meridional components, but between
296 e.g., meridional component at the first station and latitudinal component at the second station. The results for the time interval
297 8-20 UT are given in Figure 12. A high coherence ($\gamma^2>0.5$) is seen between the b_N component at VOS and b_E at DVS (Figure
298 12a) and between the b_E component at VOS and both DVS horizontal components for the 15-18 UT interval (Figure 12b).
299 Inter-hemispheric coherence over the same time interval, maximizes for the b_N components of DVS and NAL (Figure 12c).

300 The results of the coherence analysis between the pulsations in the magnetotail and those observed by ground magnetometers
301 in both the Northern and Southern polar caps show that the Pi3 pulsation recorded after 15 UT are characterized by a high
302 coherence both in a space to ground sense and also interhemispherically. A possible interpretation of this is summarized
303 below:

1) A compressional/shear Alfven wave in the magnetotail is propagating predominantly in transversal/field aligned directions, respectively. A high coherence between the pulsations observed by ground magnetometers in each polar cap demonstrate that these waves exist in both tail lobes.

2) This leads to coherent pulsations in both polar caps with a higher coherence between the meridional components for nominally conjugated positions and a higher cross-component coherence for the pulsations inside the Southern polar cap.

3.2.4 Electron density fluctuations in the ionosphere

To examine electron density fluctuations in the ionosphere over different altitudes EISCAT radar data have been used. The background Ne level was high due to Solar Extreme Ultraviolet (EUV) ionisation but the application of a low-bound filter (see sect. 2.2) allows fluctuations of electron density ΔN_e for each altitude to be calculated.

A time series of ΔN_e, centred in the F-region (at h=205 km) along with the b_N component of magnetic field at NAL is shown in Figure 13a. The spectral power of both time series is shown in figure 13b, their spectral coherence in figure 13c and the phase difference in figure 13d. The analysis indicates a common spectral maximum at f_1=1.5 mHz (Figure 13b) with a wide coherence maximum with $\gamma_{max} \approx 0.9$ (Figure 13c). The pulsations are in anti-phase with one another, as is clearly seen from both the time series and the phase-difference, which is nearly π at the f_1 frequency (Figure 13d).

Figure 14(a) shows the temporal variation of the spectral coherence, γ^2 (in the frequency band 1.2-1.9 mHz) between ΔN_e and the b_N component of the magnetic field over an altitude range covering the E and F-regions of the ionosphere (from 100 – 450km). Before 16:30 UT, the highest spectral coherence is registered with maximum at about 200 km. The same altitude of maximal coherence is seen from 16:40 until 17:30 UT. Several spots of high coherence were found at lower (~150 km centred at 17 UT) and higher (350 km around 16:30 UT and 420 km at 17-17:30 UT) altitudes. An altitude profile taken at 15:44 UT is shown in Figure 14b. Spectral coherence is high ($\gamma^2 > =0.5$) in the altitude range from 120 to 350 km, and the maximal coherence is found at $h = 205$ km. This high coherence between the geomagnetic and N_e pulsations can be a result of modulated particle precipitation. The altitudes where the highest coherence is found, correspond to the penetration altitude of electrons with energies in the hundreds of eV.

4 Discussion

Highly coherent pulsations in the Pc5/Pi3 range were observed in the magnetotail and inside the polar caps on the 8th August 2007. A spectral analysis of the IMF and SW parameters indicated that the amplitude of pulsations of a similar frequency had decreased significantly by 13:30 and 15:00 UT respectively (Figure 6). Observations made in the magnetotail (by the Cluster satellites) and in the polar caps (by ground magnetometers and the EISCAT radar) indicate that, at the same time (15 UT), the

Pc5/Pi3 ULF characteristics in this region changed. A most impressive feature of the pulsations in the magnetotail during the studied hours is a high Q factor, with a central frequency about 1.5 mHz and extremely high coherence between the two Cluster satellites. The visible pulsations are almost in-phase. At the same moment the contribution of b_ρ and b_φ (transverse) components to the total spectral power increases. The pulsations are also recorded in both polar caps by ground magnetometers. A coherence analysis shows that the maximal coherence is found for nominally conjugated positions in the magnetotail and in the southern polar cap ionosphere and between the two hemispheres for the transversal magnetic field components in the magnetotail and the b_N in the ground magnetometer data. For non-conjugated position in the same hemisphere the coherence is higher for the field-aligned component in the magnetotail and b_E in the ground magnetometer data. This could mean that the wave is a combination of a compressional mode and shear Alfven modes contributing predominantly to wave transport in transversal and parallel direction to **B**, respectively. The pulsations also show a high coherence between variations of electron concentration, ΔN_e, and the ground magnetic b_N component in the northern polar cap ionosphere. The fact that it is registered in the electron concentration could indicate modulated particle precipitation into the ionosphere from the magnetotail.

These high quality Pc-like pulsations in the magnetotail probably correspond to some resonance magnetotail mode and started after the external fluctuations had been switched off. Thus, one can speculate that usually the pulsations in the magnetotail are masked by a higher amplitude broadband ULF "noise" of extra-magnetospheric origin. The existence of quasi-resonance modes at open field lines has been discussed by previous authors, for different types of pulsations. Physically they are related to the reflection of inhomogeneities in the distribution of the Alfven velocity (e.g., Pilipenko et al., 2005). Also, as discussed by (Leonovich, and Kozlov, 2018) the laterally inhomogeneous structure of the nightside magnetosphere can also result in various resonance and waveguide MHD modes in the Pc3-6 frequency range.

It is interesting to note, that the studied event perfectly matches with the dataset used in (Yagova et al, 2017), where the authors show, that that the parameter Q is higher for pre-substorm pulsations, than for the typical polar cap Pi3s. However, given the current dataset it is not possible to conclusively link this ULF wave event to the substorm observed at 20.30UT.

5. Conclusion

- Geomagnetic pulsations with a frequency $f_1 \sim 1.5$ mHz were registered on open field lines, in both the Northern and Southern polar caps during quiet, static, space weather conditions on the 8th August 2007.

- These pulsations were also observed in the magnetotail with remarkably high quality and coherence both in space and between the magnetotail and polar cap in Earth.

- The pulsations are seen simultaneously in the ionospheric electron density enhancements in the Northern Polar Cap.

- The maximal coherence is found for nominally conjugated positions in the magnetotail and in the southern polar cap ionosphere; and between the two hemispheres for the transversal magnetic field components in the magnetotail and the meridional (b_N) component in the ground magnetometer data.

- For non-conjugated positions in the same hemisphere the coherence is higher for the field-aligned component in the magnetotail and latitudinal (b_E) component in the ground magnetometer data.

- This indicates that the wave is a combination of a compressional mode and shear Alfven modes contributing predominantly to wave transport in the transversal and parallel direction to **B**, respectively.

Data availability: Publicly available ground-based magnetometer data: IMAGE through https://space.fmi.fi/image/www/, INTERMAGNET through www.intermagnet.org. Magnetometer data from VOS station are available through (http://geophys.aari.ru) upon request. EISCAT data are publicly available through https://www.eiscat.se/scientist/data/. Cluster and OMNI data are publicly available through CDAWEB (https://cdaweb.gsfc.nasa.gov). The maps in Figure 1 are made with Natural Earth (Free vector and raster map data https://www.naturalearthdata.com).

Author contribution: NN suggested the event for the case-study, prepared ground-based data for preliminary analysis. NY developed software and performed data analysis. LB assisted with EISCAT data analysis and DL assisted with DMSP data analysis. DS provided Vostok data. The manuscript was prepared by NN and NY, after discussions with LB and DL.

Acknowledgements: The authors thank prof. V.A. Pilipenko for helpful discussions. The authors thank the institutes who maintain the IMAGE Magnetometer Array: Tromsø Geophysical Observatory of UiT the Arctic University of Norway (Norway), Finnish Meteorological Institute (Finland), Institute of Geophysics Polish Academy of Sciences (Poland), GFZ German Research Centre for Geosciences (Germany), Geological Survey of Sweden (Sweden), Swedish Institute of Space Physics (Sweden), Sodankylä Geophysical Observatory of the University of Oulu (Finland), and Polar Geophysical Institute (Russia). The results presented in this paper rely on data collected at magnetic observatories. The authors thank the national institutes that support them and INTERMAGNET for promoting high standards of magnetic observatory practice (www.intermagnet.org). The authors thank the Arctic and Antarctic Research Institute in Russia for providing ground magnetometer data from VOS station (http://geophys.aari.ru). The authors thank CDAWEB (https://cdaweb.gsfc.nasa.gov) for Cluster and OMNI data. EISCAT is an international association supported by research organisations in China (CRIRP), Finland (SA), Japan (NIPR and ISEE), Norway (NFR), Sweden (VR), and the United Kingdom (UKRI). This research was partly funded by the PolarProg and INTPART research programs under the Research Council of Norway (project numbers 246725 and 309135, NN, LB, DL) and by RFBR grant # 20-05-00787 A (NY).

The authors declare that they have no conflict of interest.

References

Allan, W., and Wright, A. N.: Magnetotail waveguide: Fast and Alfvén waves in the plasma sheet boundary layer and lobe, *J. Geophys. Res.*, 105(A1), 317– 328, doi:10.1029/1999JA900425, 2000.

Alperovich, L. S. and Fedorov, E. N.: Hydromagnetic Waves in the Magnetosphere and the Ionosphere, Series: Astrophysics and Space Science Library, vol. 353, 2009, XXIV, 418p., Hardcover, ISBN: 978-1-4020-6636-8, 2007.

Baker, G., Donovan, E. F., Jackel, B. J.: A comprehensive survey of auroral latitude Pc5 pulsation characteristics. Journ. Geophys. Res. Space Phys., 108, 1384, 2003.

Ballatore, P.: Pc5 micropulsation power at conjugate high-latitude locations, *J. Geophys. Res.*, 108, 1146, doi:10.1029/2002JA009600, 2003.

Balogh, A., Dunlop, M. W., Cowley, S. W. H., Southwood, D. J., Thomlinson, J. G., Glassmeier, K. H., Musmann, G., Luhr, H., Buchert, S., Acuna, M. H., Fairfield, D. H., Slavin, J. A., Riedler, W., Schwingenschuh K., and Kivelson, M. G.: The Cluster Magnetic Field Investigation. Space Sci. Rev., 79, 65–91, doi.:10.1023/A:1004970907748, 1997

Bland, E. C., and McDonald, A. J.: High spatial resolution radar observations of ultralow frequency waves in the southern polar cap, J. Geophys. Res. Space Physics, 121, 4005–4016, doi:10.1002/2015JA022235, 2016.

Bolshakova, O.V. and Troitskaya, V.A.: Dayside cusp dynamics from the observations of long-period geomagnetic pulsations, *Geomagn. Aeron.*, 17, 1076–1082, 1977.

Borovsky, J. E., and Denton, M. H.: Exploring the cross correlations and autocorrelations of the ULF indices and incorporating the ULF indices into the systems science of the solar wind-driven magnetosphere, Journ. Geophys. Res. Space Physics, 119, 4307– 4334, doi:10.1002/2014JA019876, 2014.

De Lauretis, M., Regi, M., Francia, P., Marcucci, M. F., Amata, E., and Pallocchia, G.: Solar wind-driven Pc5 waves observed at a polar cap station and in the near cusp ionosphere, *Journ. Geophys. Res. Space Phys.,* 121, 11,145– 11,156, doi:10.1002/2016JA023477, 2016.

Francia, P., Lanzerotti, L. J., Villante, U., Lepidi, S., and Di Memmo, D.: A statistical analysis of low-frequency magnetic pulsations at cusp and cap latitudes in Antarctica, *J. Geophys. Res.*, 110, A02205, doi:10.1029/2004JA010680, 2005.

Han, D.-S., Yang, H.-G., Chen, Z.-T., Araki, T., Dunlop, M. W., Nosé, M., Iyemori, T., Li, Q., Gao, Y.-F., and Yumoto, K.: Coupling of perturbations in the solar wind density to global Pi3 pulsations: A case study, *Journ. Geophys. Res.*, 112, A05217, doi:10.1029/2006JA011675, 2007.

Heacock, R., and Chao, J.: Type Pi Magnetic field pulsations at very high latitudes and their relation to plasma convection in the magnetosphere, *J. Geophys. Res.*, 85(A3), 1203– 1213, doi:10.1029/JA085iA03p01203, 1980.

Keiling, A., Alfvén Waves and Their Roles in the Dynamics of the Earth's Magnetotail: A Review, Space Sci Rev, 142: 73– 156, doi:10.1007/s11214-008-9463-8, 2009.

Kepko, L., Spence, H. E., and Singer, H. J.: ULF waves in the solar wind as direct drivers of magnetospheric pulsations, Geophys. Res. Lett., 29, 1197, doi:10.1029/2001GL014405, 2002.

Kepko, L., Viall, N. M., and Wolfinger, K.: Inherent length scales of periodic mesoscale density structures in the solar wind over two solar cycles. Journal of Geophysical Research: Space Physics, 125, e2020JA028037. https://doi.org/10.1029/2020JA028037, 2020.

Kozyreva, O., Pilipenko, V., Engebretson, M. J., Yumoto, K., Watermann, J., and Romanova, N.: In search of a new ULF wave index: Comparison of Pc5 power with dynamics of geostationary relativistic electrons, *Planet. Space Sci.*, **55**, 755, 2007.

Leonovich, A. S., and Kozlov, D. A.: Kelvin-Helmholtz instability in the geotail low-latitude boundary layer. Journal Geophys. Res.: Space Phys., 123, 6548– 6561. https://doi.org/10.1029/2018JA025552, 2018.

Lepidi, S., Villante, U., Vellante, M., Palangio, P., and Meloni, A.: High resolution geomagnetic field observations at Terra Nova Bay, Antarctica, Ann. Geophys., 39, 519– 528, doi:10.4401/ag-3987, 1996.

Lyons, L. R., Nagai, T., Blanchard, G. T., Samson, J. C., Yamamoto, T., Mukai, T., Nishida, A., and Kokubun, S.: Association between Geotail plasma flows and auroral poleward boundary intensifications observed by CANOPUS photometers, *J. Geophys. Res.*, 104(A3), 4485– 4500, doi:10.1029/1998JA900140, 1999.

Lyons, L. R., Nishimura, Y., , Kim, H.-J., Donovan, E., Angelopoulos, V., Sofko, G., Nicolls, M., Heinselman, C., Ruohoniemi, J. M. , and Nishitani, N.: Possible connection of polar cap flows to pre- and post-substorm onset PBIs and streamers, *J. Geophys. Res.*, 116, A12225, doi:10.1029/2011JA016850, 2011.

Mann, I.R., Voronkov, I., Dunlop M., et al., Coordinated ground-based and Cluster observations of large amplitude global magnetospheric oscillations during a fast solar wind interval. Ann. Geophys. 20, 405–426, 2002

Nishimura, Y., Lyons, L. R., Shiokawa, K., Angelopoulos, V. Donovan, E. F., and Mende , S. B.: Substorm onset and expansion phase intensification precursors seen in polar cap patches and arcs, J. Geophys. Res. Space Physics, 118, 2034–2042, doi:10.1002/jgra.50279, 2013.

Nishimura, Y., et al.: Coordinated ionospheric observations indicating coupling between preonset flow bursts and waves that lead to substorm onset, *J. Geophys. Res. Space Physics*, 119, 3333– 3344, doi:10.1002/2014JA019773, 2014.

Pilipenko, V. A., N. G. Mazur, E. N. Federov, M. J. Engebretson, and D. L. Murr, Alfven wave reflection in a curvilinear magnetic field and formation of Alfvenic resonators on open field lines, J. Geophys. Res., 110, A10S05, doi:10.1029/2004JA010755, 2005.

Pilipenko, V.A., Kawano, H., and Mann, I.R.: Hodograph method to estimate the latitudinal profile of the field-line resonance frequency using the data from two ground magnetometers. Earth Planet Sp 65, 5, doi:10.5047/eps.2013.02.007, 2013.

Posch, J. L., Engebretson, M. J., Pilipenko, V. A., Hughes, W. J., Russell, C. T., and Lanzerotti, L. J.: Characterizing the long-period ULF response to magnetic storms, *J. Geophys. Res.*, 108, 1029, doi:10.1029/2002JA009386, A1, 2003.

Rae, I.J., Donovan, E. F., Mann, I. R., Fenrich, F. R., Watt, C. E. J., Milling, D. K., Lester, M., Lavraud, B., Wild, J. A., Singer, H. J., Rème, H., Balogh. A., Evolution and characteristics of global Pc5 ULF waves during a high solar wind speed interval. J. Geophys. Res. 110, A1221, doi:10.1029/2005JA011007, 2005.

Shi, X., Baker, J. B. H.,Ruohoniemi, J. M., Hartinger, M. D., Murphy, K. R., Rodriguez, J. V., et al. Long-lasting poloidal ULF waves observed by multiple satellites and high-latitude SuperDARN radars. *Journal of Geophysical Research: SpacePhysics*, *123*, 8422–8438. https://doi.org/10.1029/2018JA026003, 2018

Shi, X., Hartinger, M. D., Baker, J. B. H., Ruohoniemi, J. M., Lin, D., Xu, Z., et al.: Multipoint conjugate observations of dayside ULF waves during an extended period of radial IMF. *Journal of Geophysical Research: Space Physics*, *125*, e2020JA028364. https://doi.org/10.1029/2020JA028364, 2020.

Wang, G. Q., Zhang, T. L., and Volwerk, M.: Statistical study on ultralow-frequency waves in the magnetotail lobe observed by Cluster, *J. Geophys. Res. Space Physics*, 121, 5319– 5332, doi:10.1002/2016JA022533, 2016.

Weatherwax, A. T., Rosenberg, T. J., Maclennan, C. G. Doolittle, J. H. : Substorm precipitation in the polar cap and associated Pc 5 modulation, Geophys. Res. Lett, 24, 579-582, 1997.

Wing, S., Sibeck, D. G., Wiltberger, M., and Singer, H.: Geosynchronous magnetic field temporal response to solar wind and IMF variations, J. Geophys. Res., 107(A8), 1–10, doi:10.1029/2001JA009156, 2002.

Yagova, N., Pilipenko, V., Rodger, A., Papitashvili, V., and Watermann, J.: Long period ULF activity at the polar cap preceding substorm, in: Proc. 5th International Conference on Substorms, St. Peterburg, Russia (ESA SP-443), 603–606, 2000.

Yagova, N. V., Pilipenko, V. A., Lanzerotti, L. J., Engebretson, M. J., Rodger, A. S., Lepidi, S., and Papitashvili, V. O., Two-dimensional structure of long-period pulsations at polar latitudes in Antarctica, J. Geophys. Res., 109, A03222, doi:10.1029/2003JA010166, 2004

Yagova N., Pilipenko, V.., Watermann, J., Yumoto, K.: Control of high latitude geomagnetic fluctuations by interplanetary parameters: The role of suprathermal ions, Annales Geophysicae, 25, 1037-1047, 2007.

Yagova, N. V., Spectral Slope of High-Latitude Geomagnetic Disturbances in the Frequency Range 1–5 mHz. Control Parameters Inside and Outside the Magnetosphere, Geomagn. Aeron., 55, 32-40, 2015

Yagova, N., Nosikova, N., Baddeley, L., Kozyreva, O., Lorentzen, D. A., Pilipenko, V., and Johnsen, M. G.: Non-triggered auroral substorms and long-period (1–4 mHz) geomagnetic and auroral luminosity pulsations in the polar cap, Ann. Geophys., 35, 365–376, doi:10.5194/angeo-35-365-2017, 2017.

Zhang, S., Tian, A., Shi, Q., Li, H., Degeling, A. W., Rae, I. J., Forsyth, C., Wang, M., Shen, X., Sun, W., Bai, S., Guo, R., Wang, H., Fazakerley, A., Fu, S., and Pu, Z.: Statistical study of ULF waves in the magnetotail by THEMIS observations, Ann. Geophys., 36, 1335–1346, https://doi.org/10.5194/angeo-36-1335-2018, 2018.

Table 1. Station coordinates and their parameters

Station code	Geographic		Geomagnetic (CGM)		UT of MLT midnight
	Latitude	Longitude	Latitude	Longitude	
NAL	78.92	11.95	76.34	110.45	20:59

LYR	78.20	15.82	75.40	111.20	20:55
HOP	76.5	25.1	73.22	114.53	20:40
TRO	69.66	18.95	66.75	102.42	21:26
THL	77.48	290.83	84.84	29.19	3:13
DRV	-66.66	140.01	-80.37	236.04	12:55
VOS	-78.46	106.82	-83.57	55.15	1:02
DVS	-68.58	77.97	-74.75	101.17	21:58

487
488
489
490
491
492

493
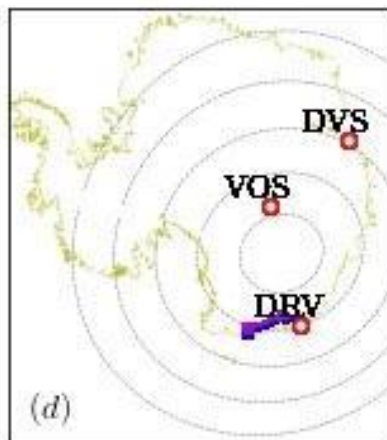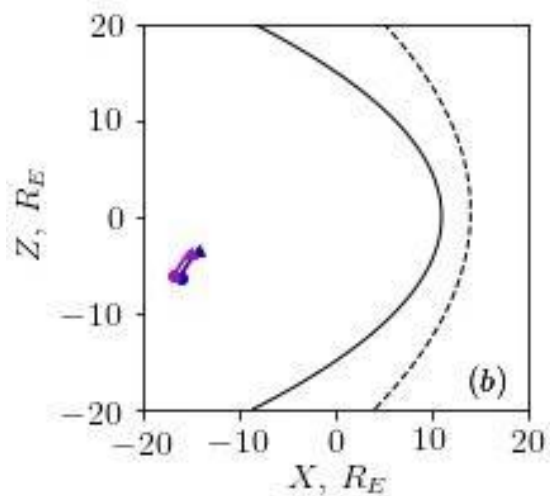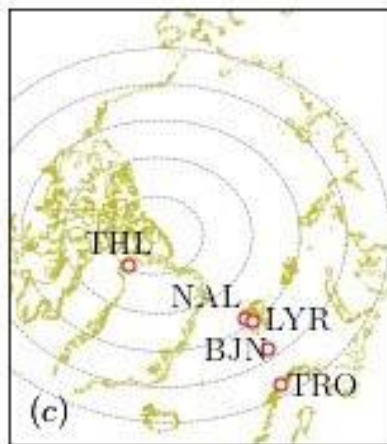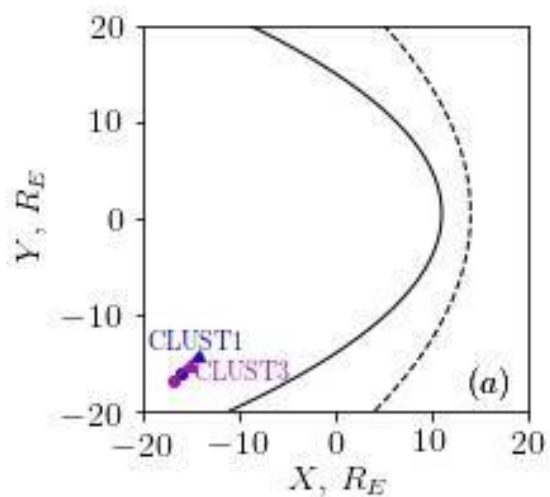
494 **Figure 1: Cluster 1 and 3 satellites orbits in GSE coordinates (XY – panel (a), XZ –(b)) and their projection on the map with**
495 **observatories located in the (c) Northern and (d) Southern hemispheres (12-18 UT). The initial point and final point are marked**
496 **with a circle and a triangle, respectively.**
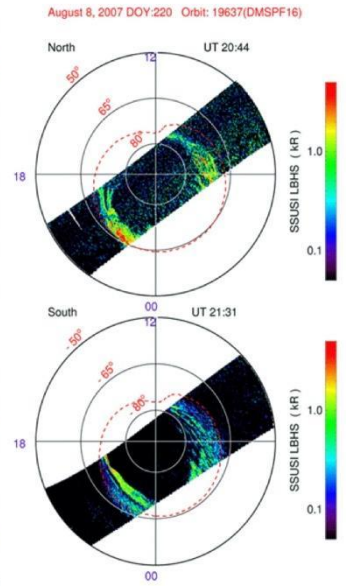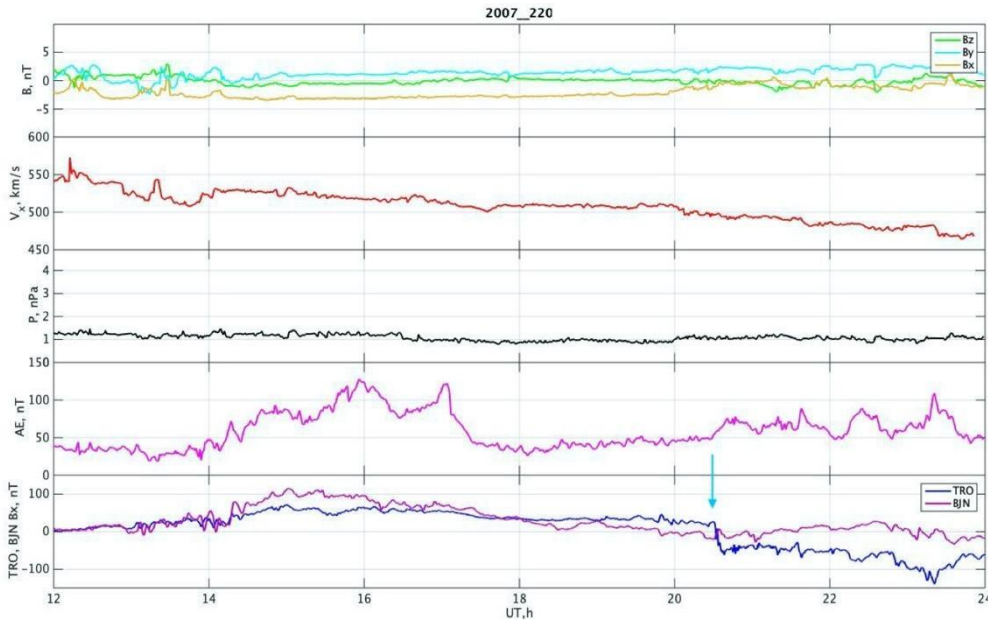
497
498 **Figure 2: The particle precipitation seen from the DMSP satellite (right panel) and the solar wind parameters as well as ground**
499 **based magnetometers data (left panel, from top to bottom: IMF all components; SW speed; SW pressure; AE-index; the magnetic**
500 **field data from the TRO and BJN stations. A small substorm is marked with the vertical blue arrow).**
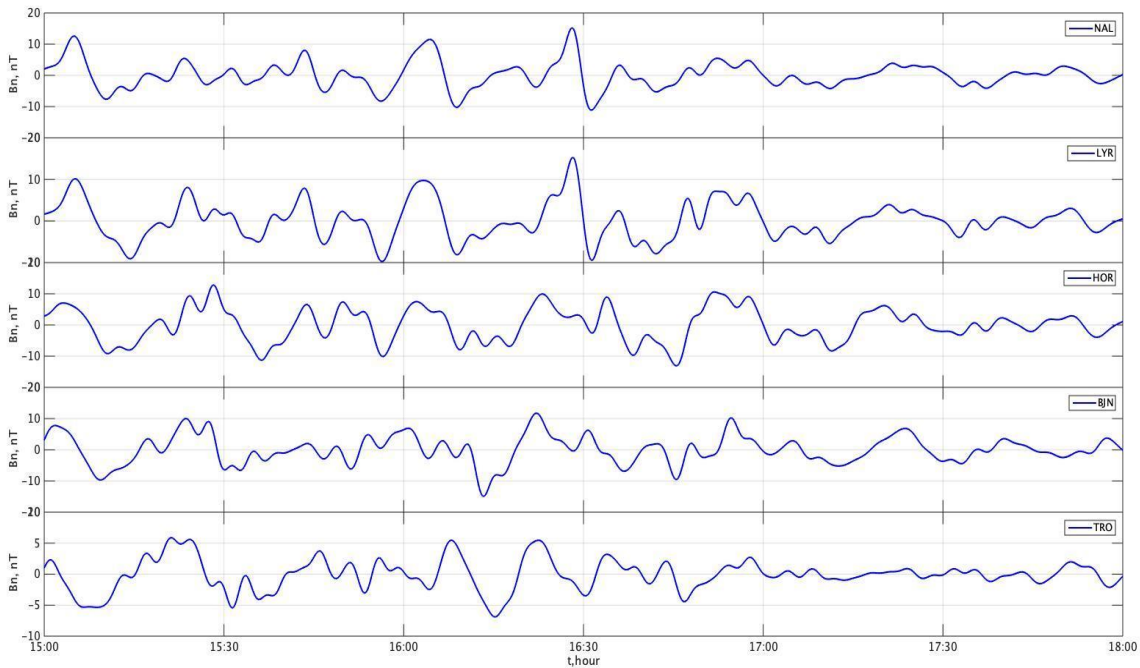
501

502   **Figure 3: A latitude profile of geomagnetic pulsations registered on Svalbard (4 top panels) and at Tromsø (the bottom panel).**

503
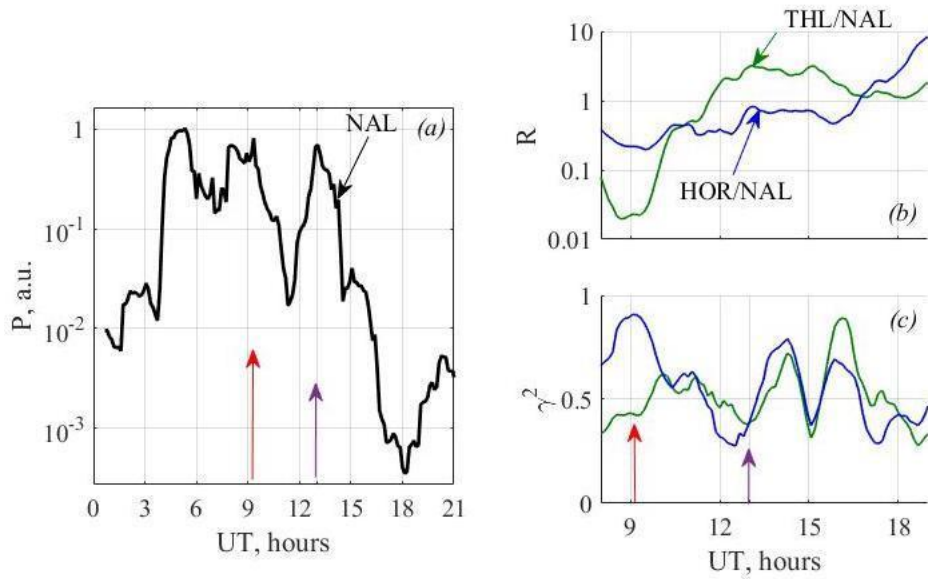
504

505   **Figure 4: (a) Diurnal variations of the spectral power in 1.2-1.9 mHz frequency band for NAL b_N component (b) PSD spectral ratio**
506   **and(c), spectral coherence for the NAL-THL and NAL-HOR station pairs. Near-noon and afternoon maxima are marked by arrows.**

507
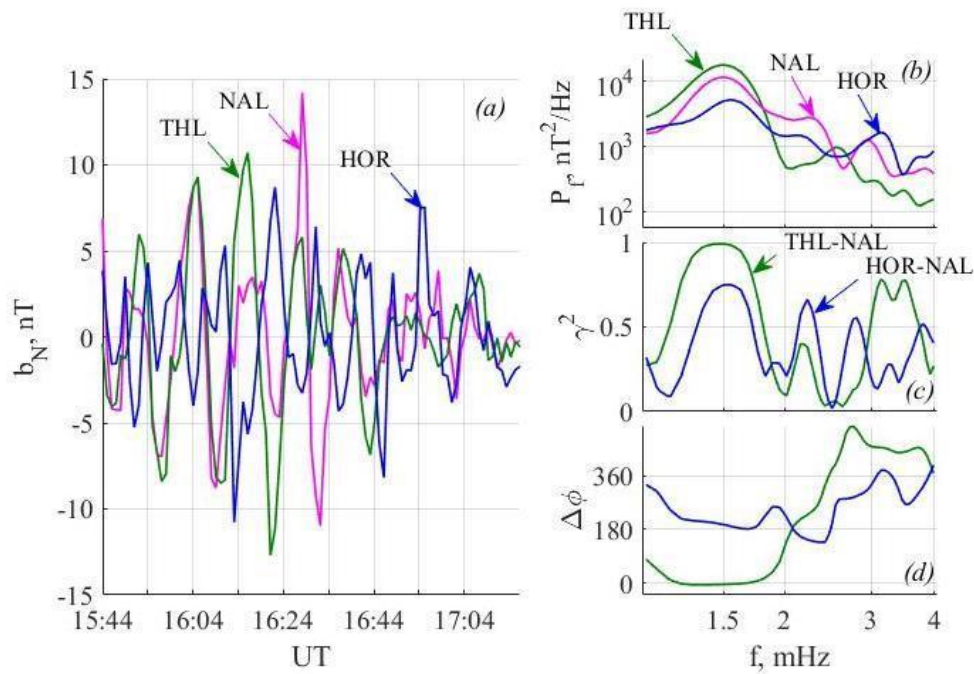
508 Figure 5: (a) Pulsations of b_N component at NAL, THL, and HOR during the interval starting at 15:44 UT; (b) PSD spectra; (c)
509 spectral coherence for THL- NAL and HOR- NAL pairs of stations; (d) phase differences. THL- NAL and HOR- NAL station pairs
510 at panels (c) and (d) are shown with the same colours as THL and HOR at panels (a) and (b).
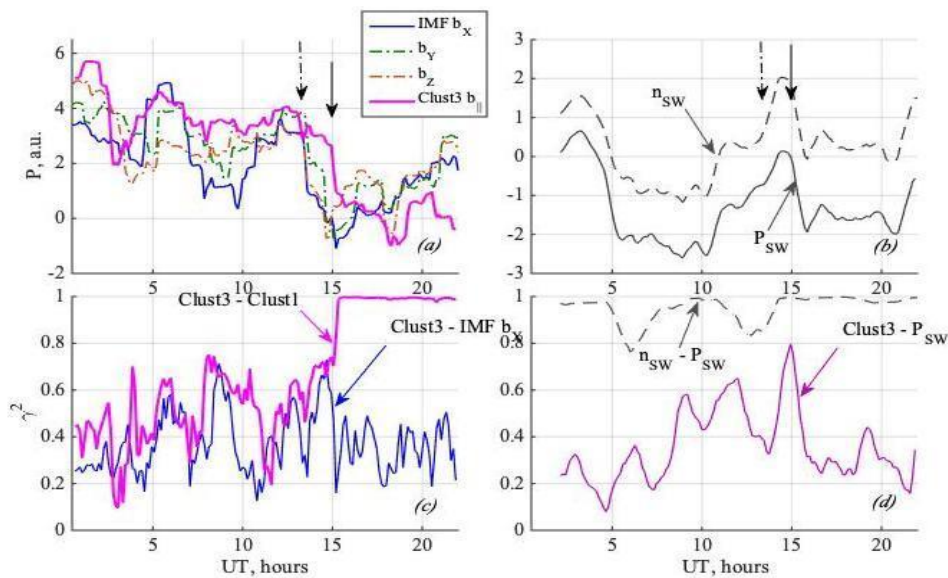
511

512 **Figure 6: Left column: Time variations of (a) spectral power and (c) average spectral coherence for the three IMF components**
513 **(GSM) and field aligned $b_\parallel$ components at Clusters 1 and 3. Right column: (b) variations of total spectral power and (d) average**
514 **spectral coherence for the SW density and SW dynamic pressure as well as field aligned $b_\parallel$ components at Clusters 3. The dot-dash**
515 **and solid arrows indicate the time at which there is a significant decrease of the spectral power in the IMF fluctuations (dot-dashed),**
516 **and in $b_\parallel$ at Cluster and the SW density and pressure (solid).**
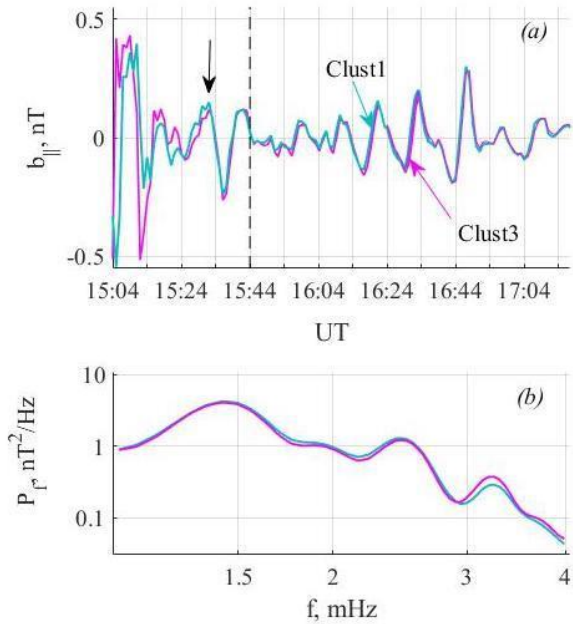
517

518 **Figure 7: (a) Pulsations of $b_\parallel$ component in the magnetotail, recorded by Clusters 1 and 3 during the interval starting at 15:04 UT;**
519 **and (b) PSD spectra for the 96-min interval starting at 15:44 (the start instant of the window, for which the spectra are calculated**
520 **is marked with a vertical dashed line). The change of pulsation regime is marked with an arrow. Pulsations at Clusters 1 and 3 are**
521 **shown with the same colours in all the panels**

522
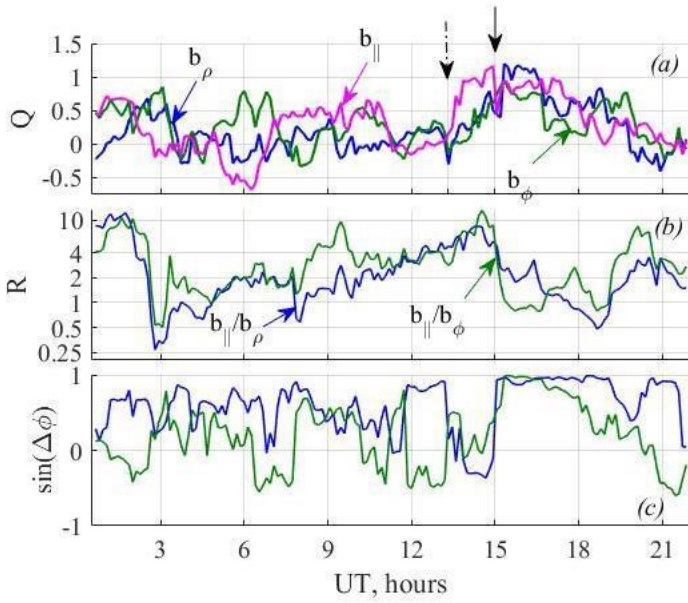
Figure 8: Time variations of (a) the parameter Q, (b) spectral field-aligned to transversal components spectral power ratio R, and (c) the sinus of phase difference at Cluster 3. The change of pulsation regime in the IMF (at 13:30UT) and in $b_\parallel$ at Cluster at 15 UT is marked by the arrows, similar to Figures 7.

526
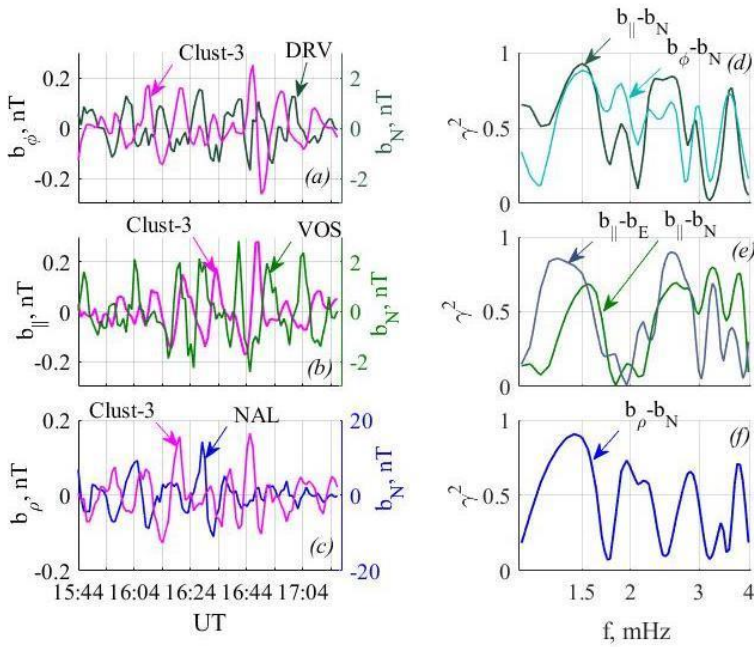
Figure 9: Pulsations in the magnetotail (Cluster-3) and of b_N on Earth. Pulsations at Cluster 3 and one of the ground stations are shown in panels (a-c). A component with the maximal coherence at the f_1 frequency with the corresponding station is shown at each of a-c panels. Left/right Y-axis correspond to Cluster 3/ground, respectively. Spectral coherence for the same satellite –station pairs are given in panels (d-f).
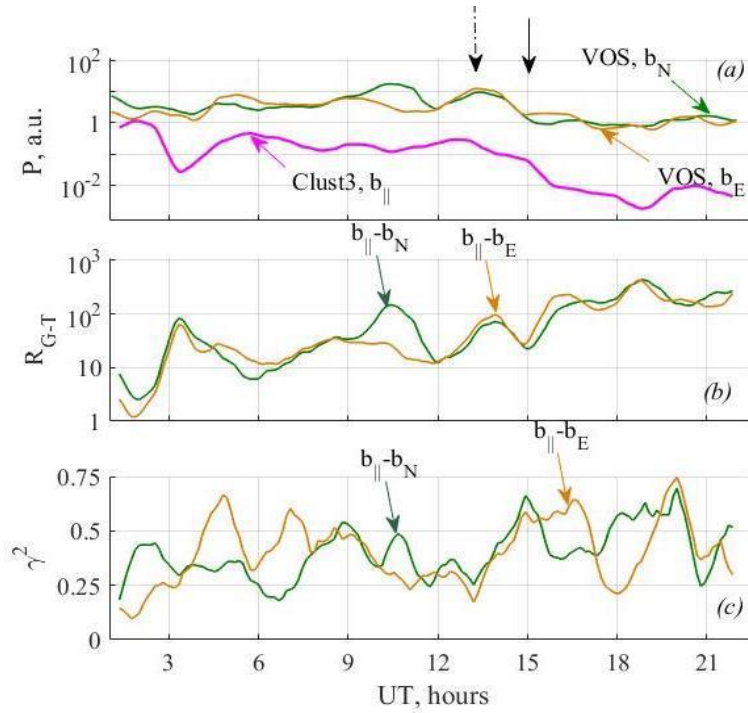
Figure 10: Time variations of (a) spectral power, (b) ground to tail spectral ratio $R_{G\text{-}T}$, and average (c) spectral coherence in the 1.2-1.9 mHz frequency band for $b_\parallel$ components at Cluster 3 and both horizontal components at VOS. Time instants of decrease of spectral power of IMF fluctuations and pulsations in $b_\parallel$ at Cluster are marked with dot-dash and solid arrows, respectively.

535
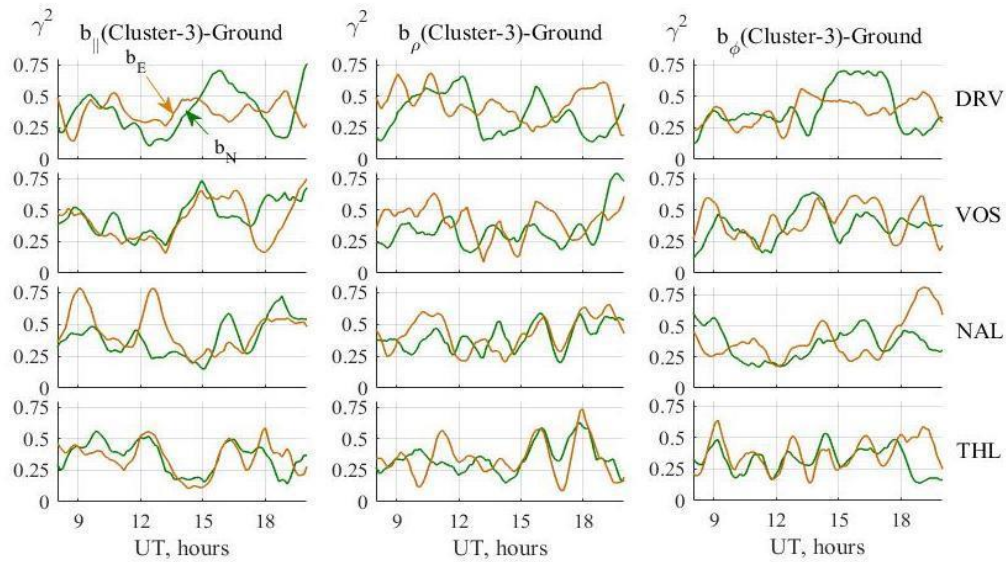
536 **Figure 11: Time variations of average spectral coherence in 1.2-1.9 mHz frequency band for all component pairs formed from**
537 **Cluster-3 and the 4 stations. 3 columns correspond to $b_\parallel$, b_ρ, and b_φ Cluster components, and the rows show the DRV, VOS, NAL,**
538 **and THL stations. The b_N and b_E components on Earth are shown in green and orange, respectively.**

539
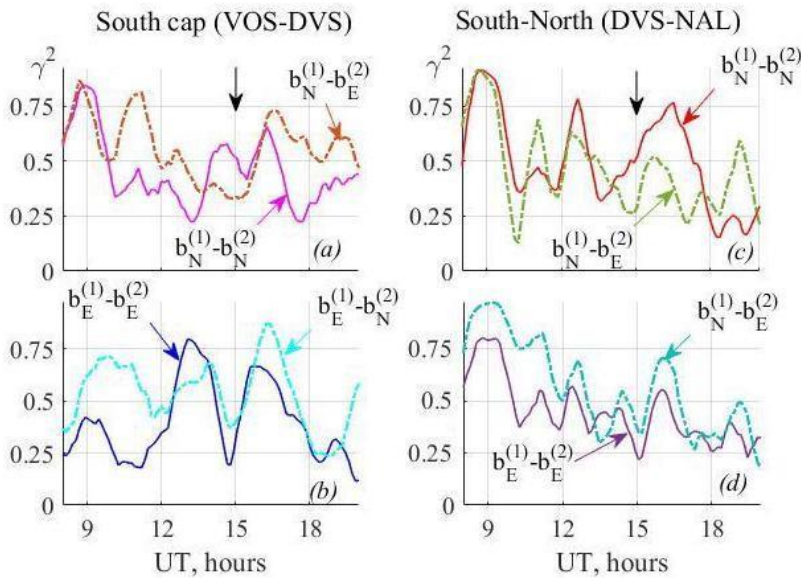
540 **Figure 12: Time variations of average spectral coherence in 1.2-1.9 mHz frequency band between two points in the Southern polar**
541 **cap and between the Southern and the Northern polar cap stations: (a) b_N component at VOS - both horizontal components at DVS;**
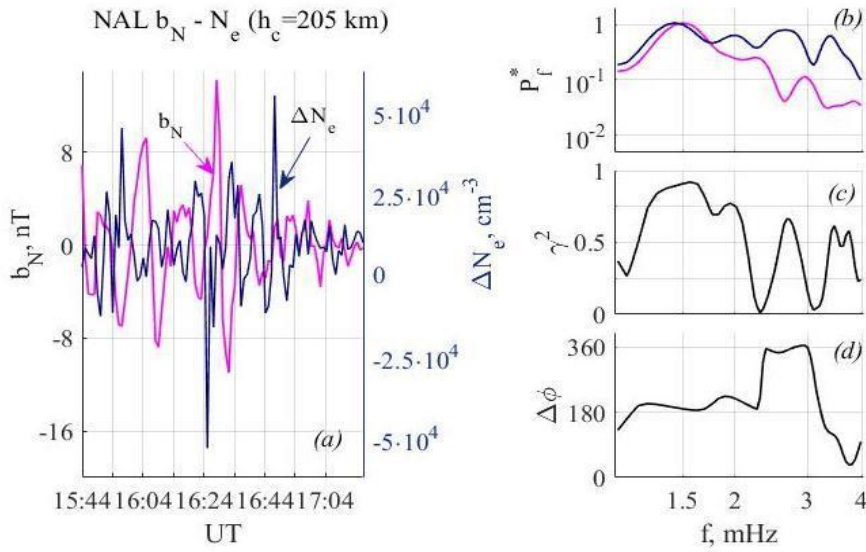
547

548 **Figure 13: (a) Pulsations of b_N component at NAL and fluctuations of N_e in the altitude band 190-220 km during the interval starting**

549 **at 15:44 UT; (b) PSD spectra; (c) spectral coherence; (d) phase differences.**

550
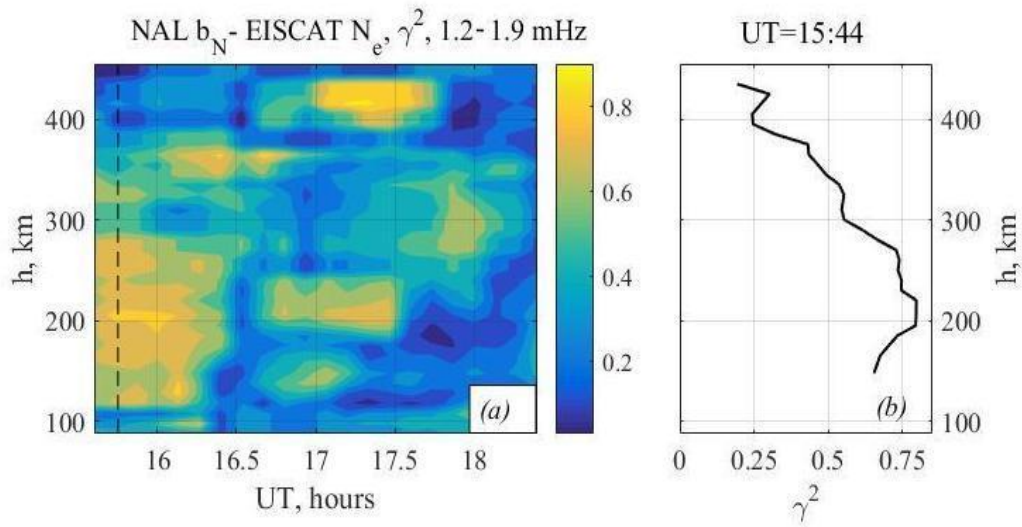
Figure 14: Dynamic altitude distribution of spectral coherence between EISCAT N_e and NAL b_N in 1.2-1.9 mHz frequency band at evening hours (a), and the altitude distribution of spectral coherence for the 15:44 interval.